A Preclinical System Prototype and Experimental Validation of Focused Microwave Brain Hyperthermia

Zijun Xi, Jiaqi Feng, Ke Ye, Dantong Liu, Xuanyu Wang, Xiaoqiang Wang, and Xiong Wang, *Member, IEEE*

***Abstract*— Focused microwave hyperthermia is a noninvasive, non-ionizing, and accurate treatment method that is promising for dealing with many kinds of cancers. Although focused microwave brain hyperthermia (FMBH) has been studied by some previous works, experimental evaluation of this technique in a practical experimental context has not been reported. This article aims to address this issue by developing a preclinical system prototype of FMBH and performing systematic experimental evaluation using several realistic head phantoms. We designed a 1.3-GHz hyperthermia applicator with 17 antennas and built nine different head phantoms based on a real human skull. We perform electromagnetic and thermal simulations and prove that the designed applicator can reliably achieve a good focused field and 45 °C temperature at the tumor. We then realize the FMBH system prototype and experimentally test the performance by applying fabricated 3-D head phantoms. The measured temperature results demonstrate that the FMBH system prototype is able to selectively treat the tumor. We also prove that the temperature at the tumor can be controlled at a constant level for a demanded time period for hyperthermia. This work provides a valuable experimental demonstration of the FMBH technique and is meaningful for its future development and clinical applications.**

***Index Terms*— Brain tumor treatment, focused microwave hyperthermia, noninvasive hyperthermia, phased antenna array.**

I. Introduction

GLIOMA is a kind of tumor originating from brain glial cells, which is the most common primary craniocerebral tumor, accounting for about 27% of all primary cerebral tumors and 80% of all malignant cerebral tumors [1]. It also has the second-highest morbidity and mortality rate [1]. At present, the clinical treatment of glioma is still mainly based on surgery and radiotherapy. However, the glioma cells usually infiltrate into the adjacent normal brain tissues, the highly irregular tumor boundaries make it difficult to completely resect the glioma without damaging the central nervous system. Accordingly, excessive bleeding during operation is very common and the recurrence rate of the tumor is high, which limits the therapeutic effect [2].

Hyperthermia is a fast-developing and increasingly used new technique in tumor treatment. It inactivates the malignant cells and achieves the goal of treatment by sufficiently heating the tumor to maintain 42 °C–45 °C [3], [4], [5]. The heat source of hyperthermia mainly includes radio frequency electromagnetic waves, microwaves, lasers, ultrasounds, and so on. Currently, laser interstitial hyperthermia has been clinically applied in neurosurgery. However, its invasiveness can cause adverse effects such as cerebral edema and epilepsy [6], [7]. Although transcranial-focused ultrasound can also perform brain hyperthermia, the severe signal distortion caused by the skull limits the applicable region in the brain. In addition, the demanded large transducer array and the associated multichannel ultrasound source are expensive [8].

Focused microwave hyperthermia technology, on the other hand, has a great potential for noninvasive, precise, and economical treatment of tumors, which has been explored to treat breast [9], [10], [11], neck [12], [13], liver [14], and bladder cancer [15]. It employs a phased array antenna to focus the radiated microwave energy at the targeted tumor by adjusting the excitation phase and amplitude of each antenna element. It is thus possible to selectively heat up and destroy the tumor tissues without damaging the healthy tissues [16]. This focusing process is also referred to as beamforming [17].

Some previous works have studied the feasibility of focused microwave brain hyperthermia (FMBH). Burfeindt et al. [18] first proposed to apply a phased array antenna composed of dipole elements to implement FMBH. Takook et al. [16] designed a spherical hyperthermia applicator at different frequencies and used a homogeneous brain model to prove that more antenna elements can lead to a better-focusing performance. Mahmoud and Montaser [19] engineered an applicator

Received 12 November 2023; revised 17 January 2024; accepted 31 January 2024. Date of publication 18 December 2024; date of current version 6 February 2025. This work was supported in part by the National Natural Science Foundation of China under Grant 61971287, in part by the Open Project of State Key Laboratory of Millimeter Waves under Grant K202207, and in part by the Double First-Class Initiative Fund of ShanghaiTech University under Grant SYLDX035 2022. *(Zijun Xi and Jiaqi Feng contributed equally to this work.) (Corresponding authors: Xiaoqiang Wang; Xiong Wang.)*

This work involved human subjects or animals in its research. Approval of all ethical and experimental procedures and protocols was granted by the Research Ethics Committee of ShanghaiTech University and the Ethics Committee of Xin Hua Hospital affiliated to Shanghai Jiao Tong University School of Medicine.

Zijun Xi, Ke Ye, Xuanyu Wang, and Xiong Wang are with the School of Information Science and Technology, ShanghaiTech University, Shanghai 201210, China (e-mail: wangxiong@shanghaitech.edu.cn).

Jiaqi Feng and Xiaoqiang Wang are with Xinhua Hospital Affiliated to Shanghai Jiao Tong University School of Medicine, Shanghai 200092, China (e-mail: wangxiaoqiang@xinhuamed.com.cn).

Dantong Liu is with the School of Information Science and Technology, School of Life Science and Technology, ShanghaiTech University, Shanghai 201210, China.

Digital Object Identifier 10.1109/TMTT.2024.3482986

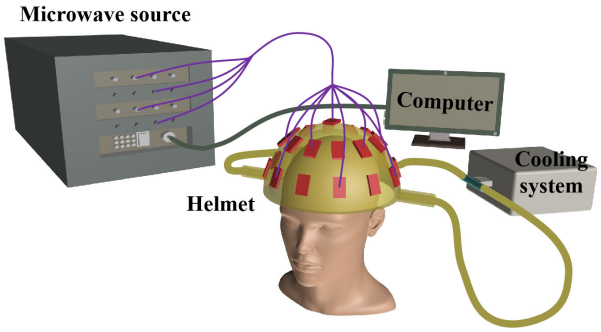

Fig. 1. Schematic of the FMBH system prototype.

made of flexible antennas and performed simulations with tumors at different locations. Redr et al. [20] studied different frequencies based on a 2-D human head model. Zanoli et al. [21] optimized the antenna distribution for a spherical applicator with ultra-wideband antennas for applications in FMBH. Hajiahmadi et al. [22] proposed a novel metasurface-based time-reversal focusing technique and obtained a sub-wavelength focal spot in a human head model. Xi et al. [23] investigated the feasibility of using microwave-induced thermoacoustic tomography (MITAT) to monitor FMBH. However, these works only provide simulation results that cannot fully recover the practical performance of the FMBH technique. Rodrigue et al. [24] reported an experimental work on FMBH, but the utilized head phantom is a simplified cylindrical model that is quite distinct from a realistic one. Therefore, validation of the FMBH methodology in a more realistic experimental context is highly desired for its future development and application.

In this study, we bridge this gap by developing a preclinical system prototype for FMBH and demonstrating the effectiveness of the system prototype by experiments. The designed FMBH system prototype is shown in Fig. 1, which mainly contains a helmet accommodating a 1.3-GHz phased array antenna, a microwave source, and a cooling system. We first carry out simulation validation of the system prototype by performing both electromagnetic full-wave simulations and thermal simulations. To increase the generality of the study, we build nine realistic inhomogeneous digital human head models with tumors of different sizes at different locations, which is rarely reported in previous works [19], [20]. The simulated results demonstrate that the microwave fields can well focus at the tumor in the brain and the temperature in the tumor can be raised by 8 °C to 45 °C in 22.5 min for tumor treatment. We then constructed an experimental FMBH system prototype to evaluate the performance by applying nine fabricated human head phantoms made from a real human skull.

As compared to previous simulation works on FMBH [16], [18], [19], [20], [21], [22], [23], the major novel contributions of this work are as follows.

1) Build a preclinical experimental system prototype to verify the FMBH technique.
2) Fabricate several inhomogeneous head phantoms for the experimental study, which have realistic anatomy and dielectric properties.
3) Investigate and compare the FMBH performance of brain tumors with different sizes at different locations.
4) Corroborate that the temperature in the brain tumor can be increased to the hyperthermia threshold without overheating in other healthy tissues.
5) Test the usefulness of the cooling system that can well cool down the scalp and cerebrospinal fluid (CSF) to avoid overheating.
6) Confirm that it is possible to maintain a constant temperature (above the hyperthermia threshold) in the tumor for a certain time (e.g., 30 min at 43 °C) [5].

As compared to previous experimental work on FMBH using a cylindrical head phantom [24], this work makes an advancement employing several 3-D inhomogeneous head phantoms based on a real human skull that is much more realistic.

II. Rationale

A. Design of FMBH System Prototype

We design a preclinical FMBH system prototype as displayed in Fig. 1. A phased array antenna mounted on a helmet radiates microwave power into the human head. A phase/amplitude tunable multichannel microwave source feeds the antennas. A cooling system serves to cool down the skin and nearby tissues. The computer controls the phase/amplitude tuning.

Compared to the breast tissues, brain tissues have generally higher conductivity, which means they are more lossy. In past studies, the most frequently used frequency in breast tumor ablation and hyperthermia is 2.45 GHz [10]. To achieve a reasonable penetration depth in the brain, for example, 4 to 5 cm, a lower microwave frequency should be used. The frequencies from 400 to 900 MHz have been applied in the applicators of FMBH [16]. Although these frequencies can penetrate deeper into brain tissues and heat deep-seated tumors, the size of the focusing spot is relatively large so small brain tumors cannot be accurately treated without burning the surrounding tissues. Therefore, the trade-off between the penetration depth and achievable focusing spot size is an important design consideration for FMBH. In this article, we choose 1.3 GHz to gain a focusing spot with a diameter of around 1.5 cm and a penetration depth of about 5 cm.

It has been demonstrated that a hemispherical antenna array is suitable for FMBH [25], [26], thus we adopt a helmet-shaped applicator with 17 bowtie-shaped patch antennas working at 1.3 GHz to form an array, as shown in Fig. 2(a). The applicator has a dimension of 27.5 × 26 × 15 cm and is fabricated by 3-D printing technique with photosensitive resin. We deploy the 17 antennas on three layers as displayed in Fig. 2(a), with 12 in layer 1, 4 in layer 2, and 1 in layer 3. Due to the limited available space on the applicator, we apply the antenna miniaturization method to reduce the dimension of the antenna to 3 × 5 cm × 3 mm, shown in Fig. 2(b). The parameters are given in Table I. The substrate of the antenna is WangLing TP-2, which is a mixture of ceramic and Polyphenylene oxide with a dielectric constant of 10.2 and a loss tangent of 0.0012 that can decrease the size

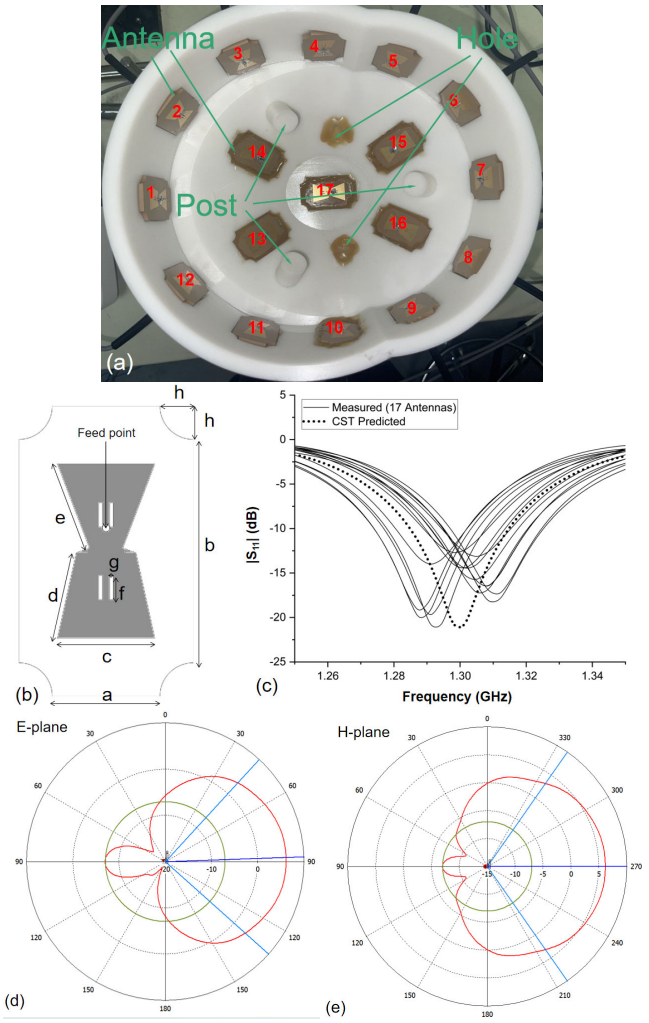

Fig. 2. Details of the designed applicator. (a) Helmet-shaped applicator, which is printed by white photosensitive resin, with 17 bowtie-shaped patch antennas. (b) Structure of the patch antenna. (c) Measured reflection coefficients for the antennas with a head phantom present. (d) and (e) Radiation pattern of the patch antenna in oil at 1.3 GHz.

TABLE I
PARAMETERS OF PATCH ANTENNA

Parameter	Value (mm)	Parameter	Value (mm)
a	18.5	e	15.43
b	38.5	f	4.17
c	16.75	g	0.6
d	15.08	h	5.75

of the antenna. We make some slots on the patch to change the distribution of surface currents and further decrease the size of the antenna. The feeding port of the antenna is a coaxial port on the back side of the patch. We fill vegetable oil between the head and applicator to play the role of coupling medium. The dielectric property of the vegetable oil is $\varepsilon_r = 3.3$ and its loss is negligible. We then optimize the antenna by CST Microwave Studio package toward acceptable performance. Fig. 2(c) shows the measured reflection coefficients for the 17 antennas with a head phantom present. It can be seen that all the antennas can obtain a -10 dB reflection coefficient at 1.3 GHz and good matching conditions are acquired. We also designed three small posts in the applicator that can hold a human head phantom and maintain a distance of about 4 cm between the antennas and the scalp, which can help to obtain a good matching condition. A multichannel microwave source feeds the antenna array through coaxial cables to provide microwave power. Both the excitation phase and amplitude of each channel can be tuned to perform beamforming in the head and focus the microwave field on the tumor.

Overheating in healthy tissues is a major problem in hyperthermia. Due to the high conductivity and microwave loss, overheating most likely occurs in the scalp and CSF. A liquid circulating cooling system, which circulates and cools down the coupling liquid, has been shown to be able to efficiently take away the accumulated heat in the scalp and nearby tissues [18], [27]. Thus, we adopt this method to avoid overheating in the scalp and CSF. We make two 1.1-cm-diameter holes on the applicator and connect them to a pump by pipelines to circulate the coupling oil, as shown in Fig. 1.

B. Basic Procedure of FMBH

The process of a clinically applicable FMBH technique can be divided into four steps. The first step is to build an accurate 3-D head model of a patient containing the accurate distribution of brain tissues and tumors by magnetic resonance imaging (MRI) or computed tomography (CT) imaging. Corresponding conductivity and permittivity values are assigned to the 3-D brain model and imported into CST Microwave Studio software. The second step is obtaining the optimal excitation phase and amplitude of antennas by an optimization algorithm to focus microwave energy on the tumor. The third step is continuously pumping microwave power to elevate the temperature in the tumor. To precisely treat the targeted tumor region, the temperature of the tumor must be enhanced to 45 °C, while the temperature of healthy tissues is maintained below 42 °C [3]. The final step is slightly turning down the excitation power level to maintain the temperature in the tumor at 45 °C and keeping this setup for about 10 min to prevent irreversible damage to the malignant tissues [28], [29].

III. SIMULATION RESULTS

A. Microwave Beamforming

We design nine inhomogeneous head models as shown in Fig. 3, which contain eight kinds of tissues. The dielectric properties of these tissues are given in Table II, which are measured from tissue-mimicking phantoms to be discussed in Section IV-A [30]. Testing several head models having a tumor at different locations with different diameters is very meaningful for evaluating the robustness and potential limitations of the FMBH technique.

As aforementioned, we need to obtain the optimal phase and amplitude for the 17 antennas before implementing the FMBH by simulations [10], [31]. We employ CST to simulate the electric field in the entire head. For each head model, in total 17 sets of simulations are carried out, with only one antenna radiating in each set. The simulated vectorial

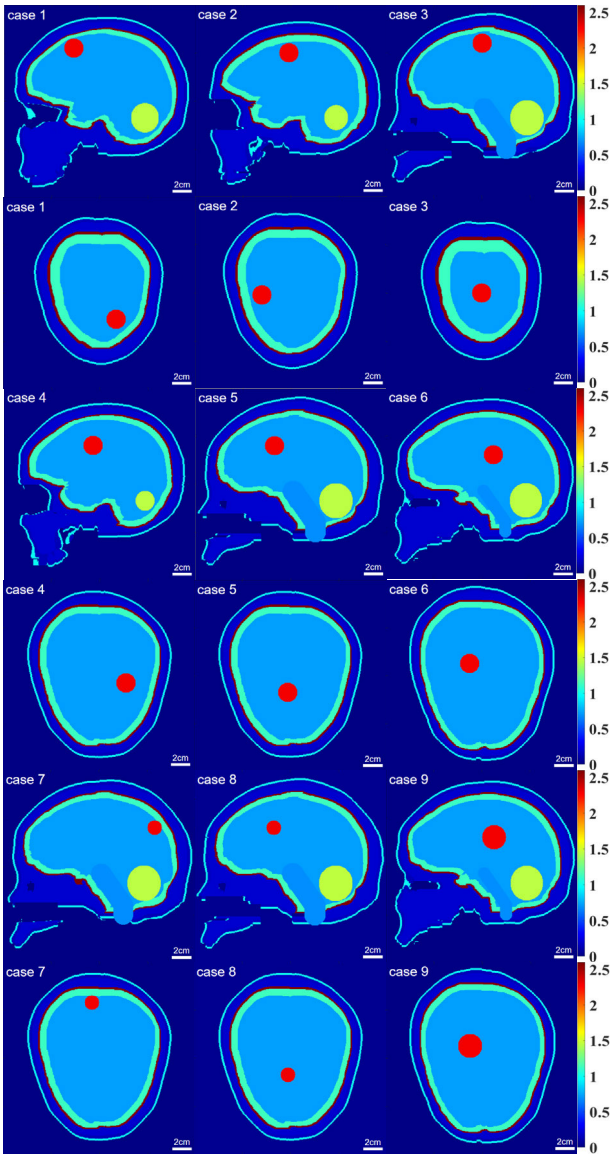

Fig. 3. Distributions of conductivity in the nine different head models in sagittal view and axial view.

TABLE II

PARAMETER OF TISSUES PHANTOM AT 1.3 GHz

Tissues	Relative Permittivity	Conductivity (S/m)
CSF	69.5	2.54
Gray matter	53.3	1.24
White matter	39.1	0.63
Tumor	68.2	2.25
Epencephalon	49.1	1.10
Brainstem	30.7	0.66

electric fields are further processed by applying the differential evolution optimization method to optimize the phase and amplitude, which is done by MATLAB [31]. The aim of the optimization is to maximize the ratio of the specific absorption rate (SAR) in the tumor to that in the healthy tissues to avoid unnecessary hot spots outside of the tumor. We adopt the cost function as

$$f = Q_{\text{tumor}}/Q_{\text{healthy}}. \tag{1}$$

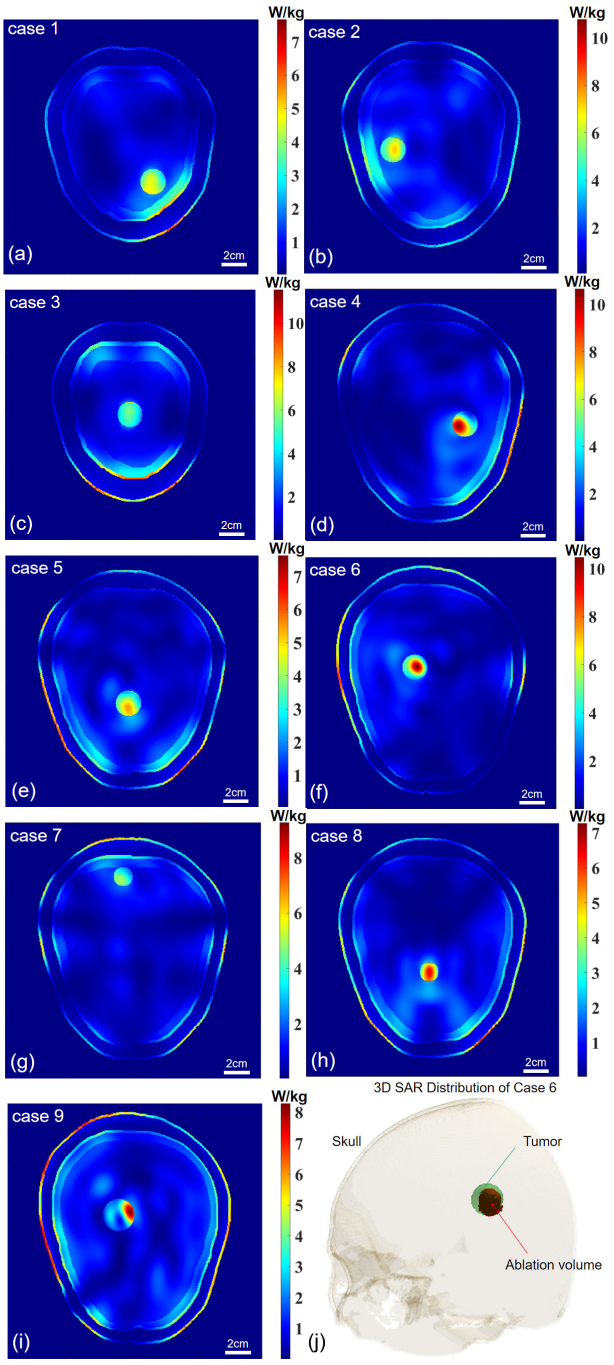

Fig. 4. (a)–(i) Axial view of the SAR distributions in the nine head models. (j) Three-dimensional SAR distribution of case 6.

Q_{tumor} means the average absorbed power in the tumor and Q_{healthy} means the maximum absorbed power in the healthy tissues in the brain. To save memory resources and computing time, we first optimize the phase by fixing the amplitude and then optimize the amplitude by using the optimized phase.

With dozens of iterations, the SAR ratio of all nine cases becomes convergent. The axial view of the synthesized optimal SAR results for the nine head models is shown in Fig. 4. The focusing spot at the tumor can be seen obviously, which proves the effectiveness of the obtained optimal microwave

beamforming. The 3-D SAR distribution of case 6 is given in Fig. 4(j), which provides a more complete view. It is also found that in many cases the high SAR can also occur in the scalp or CSF layer due to their high conductivity. The overheating in the scalp and CSF can be weakened by the circulation of the coupling liquid, to be discussed in Section III-B. It should be noted that we only need to get the microwave focusing condition (or SAR distribution) from Fig. 4 and the absolute value of SAR can be ignored for this purpose.

B. Temperature Simulation

Efficient hyperthermia of carcinoma tissues requires the temperature in the tumor to be maintained at about 42 °C–45 °C for a certain time [5]. In the meantime, other brain tissues should be controlled below 42 °C to avoid undesired damage. We perform thermal simulations based on CST to calculate the temperature in the tumor and human brain to evaluate the effectiveness and safety of the FMBH. The density, thermal conductivity, heat capacity, and thermal diffusion coefficient of all tissues are configured to guarantee the accuracy of thermal simulations [30]. The initial temperature of the entire head is set to 37 °C; while the temperature of the oil is maintained constantly to be 15 °C to mimic the cooling mechanism. The applied excitation amplitude (time-averaged power) of the 17 antennas varies from 0 to 5 W, which is proved to be reasonable in previous hyperthermia works [32], [33].

Fig. 5 displays the temperature distribution of the nine cases after the temperature in the tumor reaches 45 °C. They are respectively obtained after 990, 826, 1120, 996, 900, 1100, 870, 1350, and 740 s continuous microwave irradiation. We can see that the temperature is above 45 °C in all the tumors in the nine head models and most of the healthy tissues are under 42 °C. However, as showcased, cases 1 and 5 have relatively high temperatures in the normal brain tissues near the tumor. This is probably because the locations of these two tumors make it difficult for the antenna array to form a focused field. To be more specific, tumor 1 is close to the top of the head, and tumor 5 is very deep in the brain. The overheating of the healthy tissues can be solved by increasing the excitation microwave power and shortening the heating time.

According to [5], the suggested temperature rise every 5 min is 0.6 °C to 2 °C. This means the temperature rise of 8 °C should be achieved in more than 1200 s. In our tested cases, the heating period from 37 °C to 45 °C in simulations is from 740 to 1350 s. Most of the cases lead to a faster temperature rise speed than the suggestion in [5]. But this is not problematic, since the temperature rise can be simply made slower by simply using lower microwave power.

According to [34], when the blood flow is not considered, the hot spot generated by the CSF will be overestimated, and the CSF is the tissue with the highest conductivity in the brain tissue, so the temperature rise of the CSF should be avoided as much as possible. To make the setup more consistent with that in the experiments (no blood flow), the temperature change caused by the blood flow is not considered in the simulations. It is possible to consider the effects of blood flow and set the blood flow coefficient in CST in our future study.

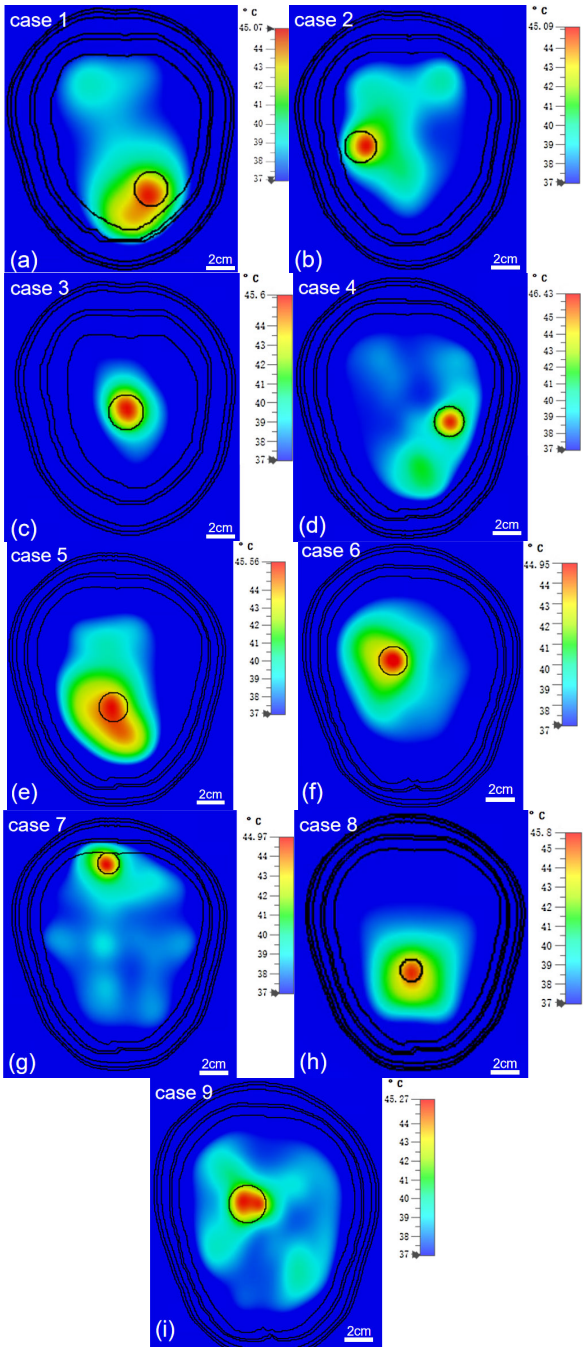

Fig. 5. (a)–(i) Axial view of the temperature distributions in the nine-head models. The diameters of the tumors in (a)–(f), (g)-(h), and (i) are respectively 2 cm, 1.5 cm, and 2.5 cm.

IV. Experimental Results

A. Phantom Preparation

We perform experimental tests to validate the FMBH technique using a head phantom containing a tumor. We use a real human skull to make a head phantom, as shown in. We obtain the 3-D structure of the skull by CT. Although a skull phantom can be made by some methods like 3-D printing [35], [36], utilizing a real human skull that maintains

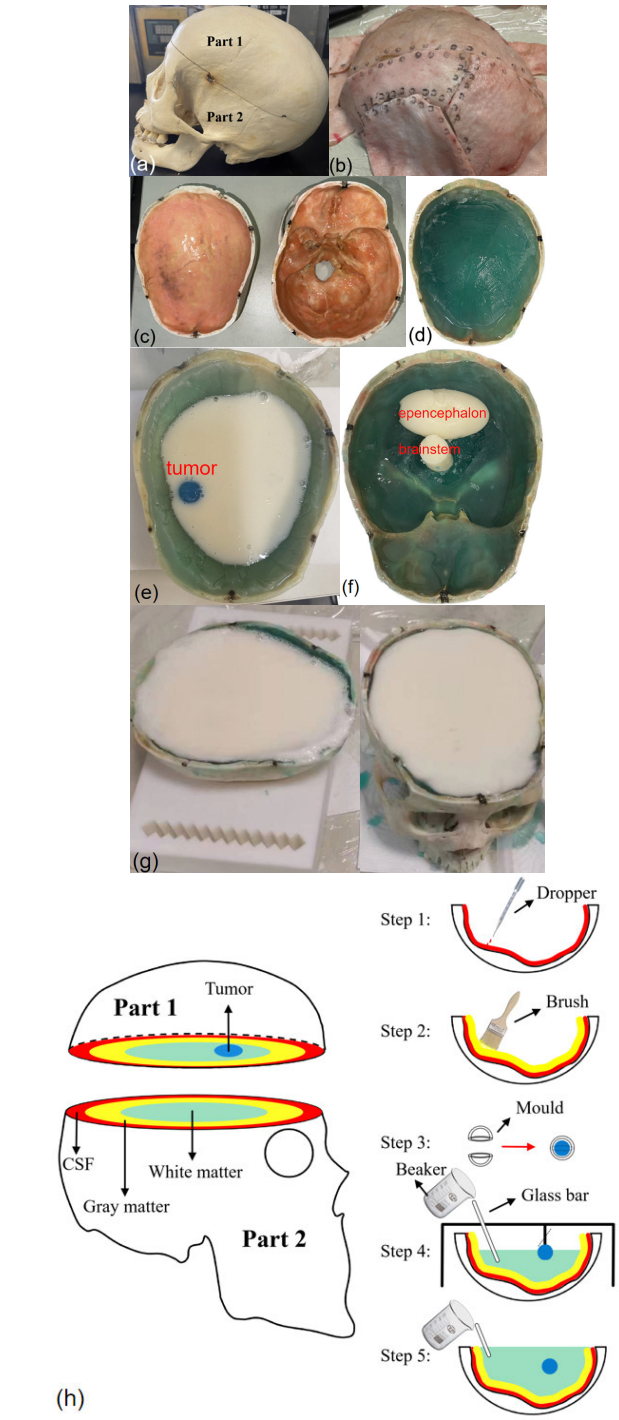

Fig. 6. Fabrication procedure of the head phantom using a real human skull. (a) Photograph of the skull that is split into two parts. (b) Porcine skin covering the skull serves as the scalp. (c) CSF phantom layer. (d) Gray matter phantom layer. (e) White matter phantom layer and the tumor phantom. (f) Epencephalon and brainstem phantoms. (g) Final fabricated two parts of the head phantom. (h) Schematic of the complete procedure of phantom fabrication.

the complicated inhomogeneous dielectric property and porous feature can better mimic a realistic case. We split the skull into two parts along the forehead and filled brain tissue phantoms into two parts, as displayed in Fig. 6(a). We attach a layer of 5-mm-thick pig skin to the outer surface of the skull to serve as the scalp, showcased in Fig. 6(b).

TABLE III
RECIPE OF BRAIN TISSUE MIMICKING PHANTOM MATERIALS IN WEIGHT

Materials	CSF	Gray matter	White matter	Tumor	Cerebellum	Brainstem
Oil	14	12	27	0	27	46
Water	68	59	46	83	60	45
Glycerin	3	17	18	0	0	0
Salt	1	0	0	1	0.3	0
Formalin	2	2	1	2	2	1
Gelatin	12	10	8	0	10	8
Agarose	0	0	0	14.	0	0

We make brain tissue phantoms and fill them into the skull to mimic a human head. In total six kinds of tissue phantoms, including the CSF, gray matter, white matter, epencephalon, brainstem, and tumor, are made of a mixture of several materials with different recipes as listed in Table III. The phantom materials are originally in the form of glutinous liquid, while gradually solidifying into semisolids. A 3 mL formaldehyde solution is put into every 100 mL phantom liquid to stiffen the phantoms and increase the melting point [37], [38]. Adding formaldehyde solution does not significantly change the dielectric properties of the phantom material. We measure the dielectric properties of the phantoms at 1.3 GHz using a coaxial dielectric probe (Keysight, N1501A). We make the end of the probe tightly touch the flat surface of the solidified phantom and connect the other end of the probe to a network analyzer that measures the S_{11} parameter. The obtained permittivity and conductivity results are tabulated in Table II, which have very good accuracy as compared to those in the literature [30].

Since the complicated structures of the cerebral gyrus of a human brain are hard to realize using phantoms, we make a head phantom with simplified boundaries of brain tissues, which bear high similarity to those in Fig. 3. First, we put a 3-D-printed mold in part 1 of the skull, which results in a 0.5- to 1-mm-thick gap between the skull and the mold. The surface of this mold represents the simplified boundary of the gray matter. We fill the CSF-mimicking liquid into this gap, which forms the CSF layer after solidification, which can be seen in Fig. 6(c). Second, after removing the first mold, we put a second mold in the skull to make a 5-mm-thick gray matter layer in a similar way to the first step, shown in Fig. 6(d). Third, we make a spherical tumor phantom. We make nine phantoms containing a tumor with different diameters (1.5, 2, and 2.5 cm) at different locations, which are given in Fig. 4. The distance from the center of the tumor to the skin varies from 2.3 to 5.4 cm. Fourth, after the gray matter and tumor are solidified, we hang the tumor phantom at its designed location and pour white-matter-mimicking liquid into the skull, shown in Fig. 6(e). Last, the epencephalon and brainstem phantoms are also produced by specifically designed molds and put in part 2 of the skull, as displayed in Fig. 6(f). The fabricated two parts of the head phantoms are given in Fig. 6(g). A schematic showing the complete procedure of phantom fabrication is given in Fig. 6(h).

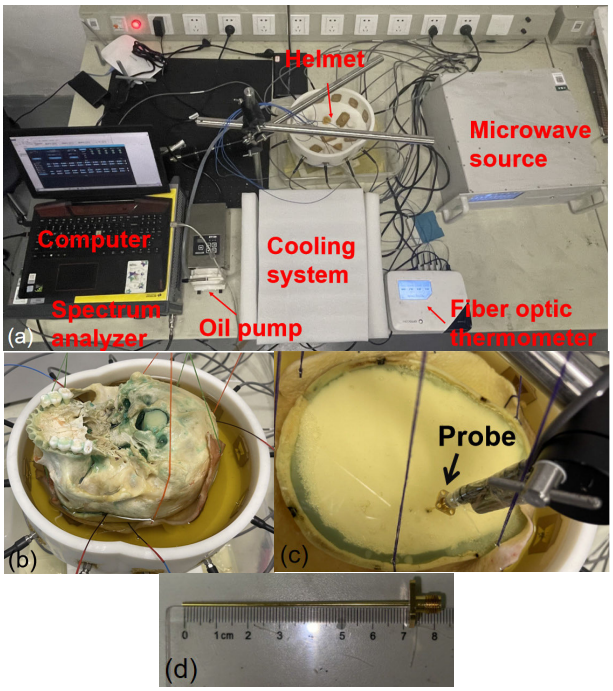

Fig. 7. Experimental setup. (a) Photograph of the developed FMBH system prototype. (b) Head phantom located in the helmet. (c) Probe inserted into phantoms to measure the absorbed power. (d) Photograph of the coaxial probe.

B. Hyperthermia Experiments

A photograph of the experimental system is shown in Fig. 7(a). The 1-cm-thick applicator is fabricated by polymer using the 3-D printing technique, which has 17 holes to accommodate the antennas. The patch antennas are mounted on the applicator using hot melt adhesive. The microwave source is produced by Amplivisions Company Ltd. It has in total of 20 channels and the maximum output power of each channel is 500 W at 1.3 GHz. The phase shifters are integrated in the microwave source and the phase tuning step or accuracy is 2.8°. The duty cycle can be tuned from 0.01% to 5% and the pulsewidth can be changed from 0.5 to 5 μs. By setting a duty cycle of 1%, we can get a maximum time-averaged power of 5 W. Low-loss flexible coaxial cables are used to connect the microwave source to the antennas. Vegetable oil is filled into the applicator. We circulate the oil by pumping it into two pipelines and putting the pipelines into a tank with an ice water mixture. The pumping speed is 570 mL/min. The temperature of the oil in the applicator can be maintained around 15 °C with a room temperature of 22 °C∼25 °C.

We put the two parts of the head phantom on the three posts in the applicator as shown in Fig. 7(b). The excitation phase/amplitude for the microwave source is determined based on the optimal phase/amplitude obtained from the simulation beamforming in Section III-A. Since the experimental system has some differences from the simulation setup, we need to slightly adjust the phase/amplitude to maximize the field at the tumor in experiments. We use a long coaxial probe connected to a spectrum analyzer (Keysight, N9010B) for this purpose [10], displayed in Fig. 7(c). The measured data by the spectrum analyzer can indicate the field strength around the tip. Specifically, we insert the probe [Fig. 7(d)] into the head phantom and put its tip at different locations, including one at the center of the tumor and some around the tumor (2∼3 cm from the center). We adjust the phase/amplitude of the 17 channels toward the goal of making the field at the center of the tumor greater than those at the locations around the tumor. We use the associated control software of the microwave source and change the phase/amplitude values on the computer. After changing the phase/amplitude, we check the result on the spectrum analyzer by placing the probe at the center of the tumor and the locations around the tumor. When the center of the tumor leads to higher power absorption than its nearby region, we can efficiently establish a focused field at the tumor.

During the hyperthermia experiment, we use a fiber optic thermometer (OPTOCON, FTT0072) to continuously measure the temperature at different locations, including the center of the tumor, the edge of the tumor, the CSF underneath the forehead, and the CSF underneath the occipital bone. Since the 0.4-mm-diameter fibers are very thin, they cause small field perturbations when inserted in the phantom materials.

The measured temperature versus time is shown in Fig. 8. Because the initial temperature of the phantom is the room temperature 22 °C∼25 °C rather than the body temperature 37 °C, it takes more time to reach 45 °C in the tumor than in those cases in the simulations. It is seen that the tumors in all nine cases can be heated up to 45 °C in about 30 to 50 min. The temperature at the edge of the tumor is a little lower than that at the center of the tumor, demonstrating the well-focused field of the tumor. The temperature in the measured two points in the CSF is generally under 35 °C, which proves the efficiency of the oil cooling mechanism. For cases with tumors at the same location but different tumor diameters, the larger tumor results in a faster temperature rise speed, e.g., case 5 is faster than case 8, and case 9 is faster than case 6. This is probably because a larger tumor absorbs more power and has a better heat confinement ability than a small tumor. Since the cooling effect can be weakened by the temperature rise in the ice-water mixture, the measured temperature increases faster than that in the simulations. In addition, it is seen that cases 1 and 3 also take longer time to reach 45 °C than some other cases. The possible reason is that the 12 antennas in layer 1 are not directly facing the tumor, so the resulting focusing effect is a little worse.

The applied optimal excitation phase/amplitude for case 6 is given in Fig. 9 as an example. It is seen that the radiated time-averaged power of some antennas is much lower than 5 W. This is because these antennas are relatively farther from tumor 6 and using a low excitation power for these antennas can help to reduce undesired hot spots in the brain, which has been reported in previous hyperthermia work [27].

In practical hyperthermia, the temperature at the tumor needs to be maintained above 45 °C for about 10 min to sufficiently damage the tumor cells [39], [40]. Thus, we need to reduce the excitation microwave power once the temperature in the tumor reaches 45 °C to avoid further temperature rise

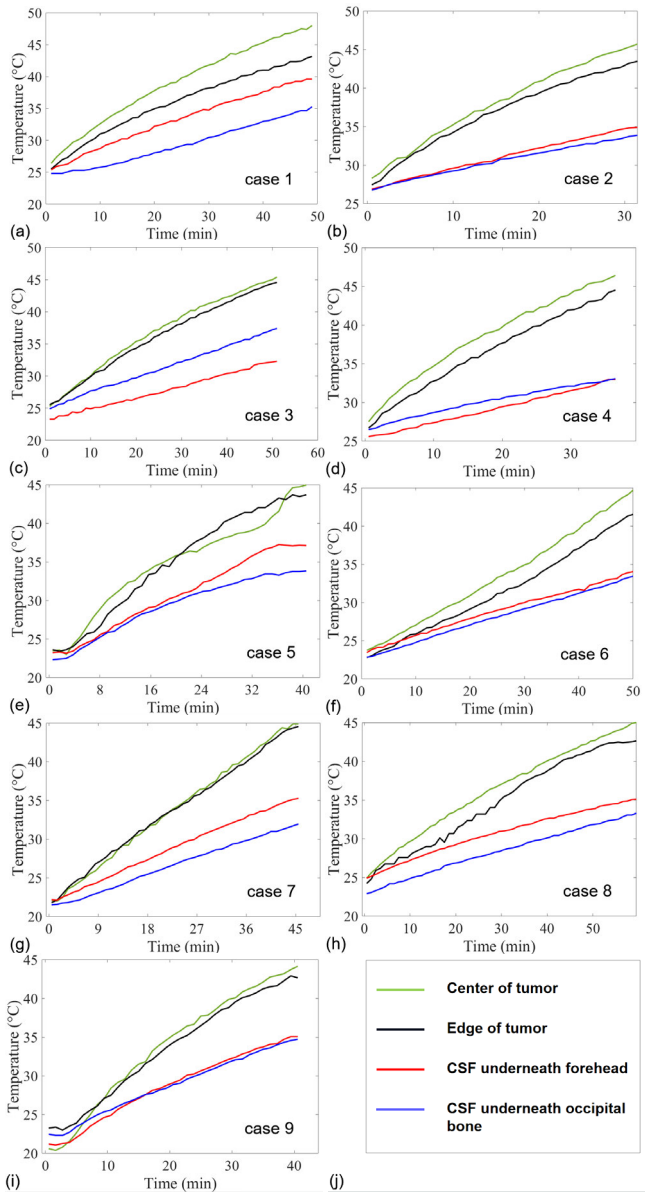

Fig. 8. (a)–(i) Measured temperature versus time at different locations of the nine cases. (j) Legend of the subfigures.

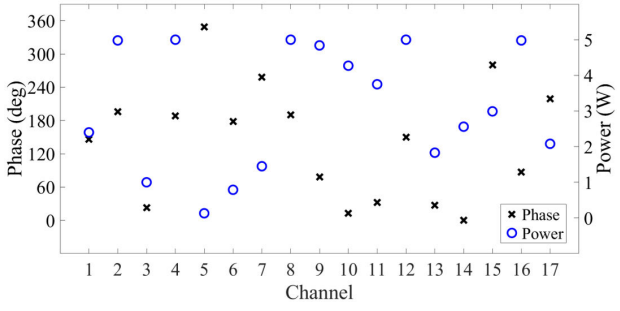

Fig. 9. Optimal excitation phase/amplitude for case 6.

in the tumor. We further conduct an experiment using the head phantom of case 6 to show the effect. After using the power in Fig. 9 to raise the temperature in the tumor to 45 °C at 49 min, we reduce the excitation power of all the antennas by 3.52 times and maintain this setup by 16 min.

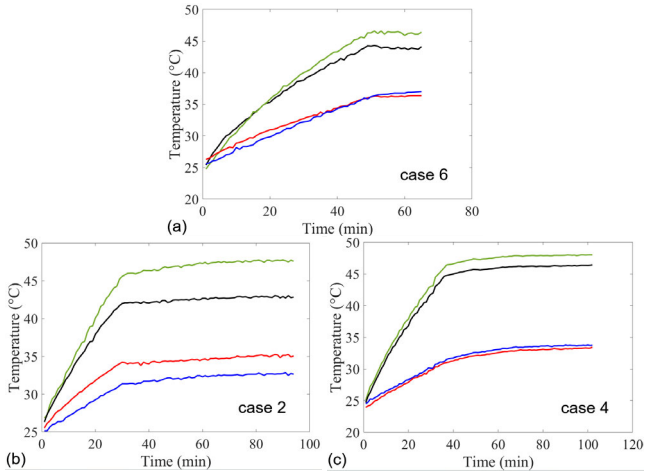

Fig. 10. (a)–(c) Measured temperature versus time for cases 2, 4, and 6, respectively, using the excitation power that can maintain the temperature in the tumor around 45 °C.

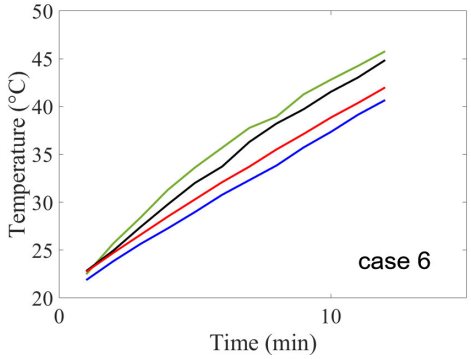

Fig. 11. Measured temperature versus time for case 6 using a 5% duty cycle.

The measured temperature is plotted in Fig. 10, which shows that the temperature in the tumor can be well controlled around 45 °C from 49 to 65 min. This result demonstrates that it is possible to maintain a constant temperature in the tumor for a required time period. For the head phantoms of other cases, it is also possible to obtain similar results by reducing the excitation microwave power. It should be noted that the part in Fig. 10(a) before 49 min is a little different from that in Fig. 8(f). This is mainly because the initial temperature (room temperature) of these two sets of experiments has a 2 °C difference and there are some small errors in making the two phantoms. Furthermore, the measured temperature curves of cases 2 and 4 are given in Fig. 10(b) and (c), which show that constant temperature for 60 min can be obtained for both cases. This means controlling the time and maintaining a constant temperature is very flexible for practical applications.

For the current preliminary proof-of-concept demonstration, we set the duty cycle of the pulsed microwave signal to 1%. By increasing the duty cycle to 5%, the excitation time-averaged power is increased by five times and the temperature can rise at a much faster speed. We still use the head phantom of case 6 for this set of experiments. As shown in Fig. 11, the temperature in the tumor can reach 45 °C in about 12 min, which can shorten the operation time

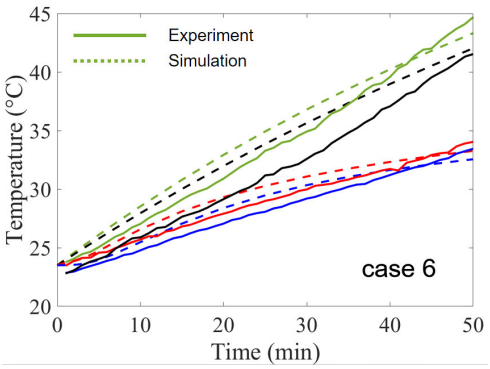

Fig. 12. Comparison of measured temperature versus time for simulation and experiment of case 6.

of the hyperthermia and reduce the potential risks of patient's movement and uncomfortableness. The reason why the CSF can be heated up to a higher temperature than that using a 1% duty cycle is because the cooling efficiency of the oil is worse in a shorter time.

We also plot the temperature versus time curve of the simulation result for case 6, as shown in Fig. 12. The simulated and measured curves have acceptable agreement. The differences between them may be due to the discrepancy between the simulation and experiment setups. First, the pig skin in experiments is thicker than the scalp in the simulations. Second, due to the toughness of the pig skin, it does not fit perfectly to the surface of the human skull. The oil can then fill in the gap between the pig skin and the skull, causing some differences from the simulation setup.

These experimental results preliminarily corroborate that our designed FMBH system can selectively elevate the temperature in the tumor to the hyperthermia threshold and ensure the safety of other tissues. The results of the nine cases can not only prove the robustness of the designed FMBH system for treating tumors at different locations but also reveal some differences among the tested cases. This is very meaningful for potential advancement and clinical applications of the FMBH method.

C. Discussions

Although we only demonstrate the performance of the FMBH system based on simplified homogeneous head phantoms, the tumors embedded in a realistic complicated human brain can also be selectively headed up by our system. We perform simulations using a realistic human brain and find that the field distributions in the brain are more complicated than the simplified brain models. However, acceptable focused fields at the tumor and selective heating of the tumor can still be obtained. The heat accumulated in the scalp can be taken away by the cooling mechanism.

The 17-antenna applicator can acquire acceptable microwave-focusing results for different head phantoms. To further improve the accuracy of focusing and shorten the heating time, increasing the number of antennas is a possible way. However, more antennas demand more channels on the microwave source which can greatly increase the cost of the system. More antennas also make the spatial distribution of antennas more crowded, which may lead to high mutual coupling between antennas [41].

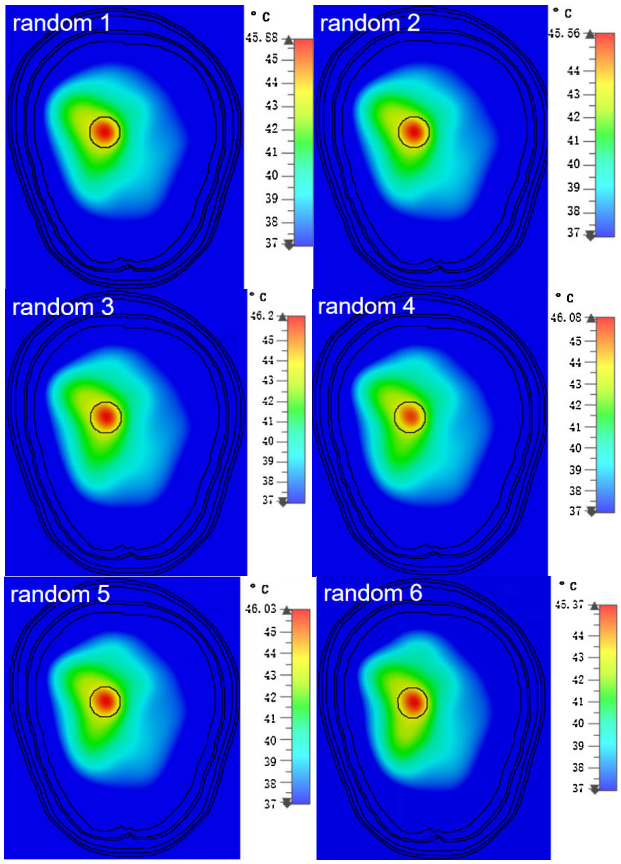

Fig. 13. Axial view of temperature of tumor 6 in the head with phase uncertainty.

Considering the phase of a multichannel microwave source may not be very accurate due to interference between channels, we study the effect of phase uncertainties on the performance of FMBH. We do a simulation for this task using the head model of case 6. We add a random disturbance of up to 15° to the optimized phase of the 17 antennas. We do six sets of simulations with different phase randomness and obtain the temperature distributions as given in Fig. 13. It is observed that they have a high resemblance to Fig. 5(f). Therefore, such phase uncertainty does not jeopardize the overall performance of the FMBH technique and proves the stability of this technique. This is similar to the case reported in our previous work for focused microwave breast hyperthermia [31].

In a practical application scenario, applying the coupling oil in the current manner may be problematic. A possible solution is deploying a flexible oil bag, similar to a water bag utilized in high-intensity focused ultrasound (HIFU), between the applicator and scalp.

For practical applications, a monitoring method to guide the beamforming is in demand to guarantee the accuracy of the FMBH technique. MITAT has been explored to monitor focused breast hyperthermia since MITAT can reconstruct the microwave power distribution in the human body [10], [42]. It is possible to use MITAI for the brain is still a challenging work. However, due to the high acoustic inhomogeneity of the

human skull, deep learning has to be applied to obtain good imaging quality [43], [44].

Besides the monitoring of the microwave-focusing condition, monitoring of the temperature in the tumor and brain during hyperthermia is also necessary to guarantee the safety and effectiveness of the FMBH technique. MRI is currently the most mature technology for noninvasive temperature measurement, which has already been researched to guide HIFU [45], [46]. For a potential MRI-guided FMBH modality, it is imperative to make the antenna array and coaxial cables to be MRI-compatible [47], [48].

V. Conclusion

We designed a preclinical system prototype for the FMBH modality, which has a helmet supporting a phased array with 17 patch antennas and a cooling system circulating the coupling medium. By building nine realistic head models with brain tumors, we perform simulations to implement beamforming and prove good microwave focusing and selective heating of the tumors. Based on a constructed system prototype and fabricated head phantoms, we experimentally evaluate the feasibility of the FMBH technique by measuring the temperature at different locations in the phantoms. First, we show that the temperature in the tumor can be elevated to 45 °C while the temperature in other tissue phantoms can be controlled below 42 °C. Second, we prove the effectiveness of the cooling system in cooling down the CSF. Third, we find that a larger tumor can be heated up faster. Fourth, we reveal that it takes a longer time to heat a tumor that cannot be directly radiated by the antennas. Fifth, we demonstrate that it is possible to maintain the temperature in the tumor at 45 °C for 60 min that is meaningful for clinical applications. Last, we prove that small uncertainties in the antenna phase do not jeopardize the performance of the FMBH system. These findings can prove the validity of the developed FMBH preclinical system prototype. We also discuss some potential directions to further improve the system. This work experimentally verifies the feasibility of the FMBH technique and is meaningful for its future applications.

References

[1] J. A. Schwartzbaum, J. L. Fisher, K. D. Aldape, and M. Wrensch, "Epidemiology and molecular pathology of glioma," *Nature Clin. Pract. Neurol.*, vol. 2, no. 9, pp. 494–503, Sep. 2006.

[2] S. Tamai et al., "Tumor microenvironment in glioma invasion," *Brain Sci.*, vol. 12, no. 4, p. 505, Apr. 2022.

[3] M. H. Falk and R. D. Issels, "Hyperthermia in oncology," *Int. J. Hyperthermia*, vol. 17, no. 1, pp. 1–18, Jan. 2001.

[4] H. H. Kampinga, "Cell biological effects of hyperthermia alone or combined with radiation or drugs: A short introduction to newcomers in the field," *Int. J. Hyperthermia*, vol. 22, no. 3, pp. 191–196, Jan. 2006.

[5] G. Bruggmoser et al., "Guideline for the clinical application, documentation and analysis of clinical studies for regional deep hyperthermia," *Strahlentherapie und Onkologie*, vol. 188, no. S2, pp. 198–211, Sep. 2012.

[6] A. A. Kamath et al., "Glioblastoma treated with magnetic resonance imaging-guided laser interstitial thermal therapy: Safety, efficacy, and outcomes," *Neurosurgery*, vol. 84, no. 4, pp. 836–843, Apr. 2019.

[7] J. Torres-Reveron, H. C. Tomasiewicz, A. Shetty, N. M. Amankulor, and V. L. Chiang, "Stereotactic laser induced thermotherapy (LITT): A novel treatment for brain lesions regrowing after radiosurgery," *J. Neuro-Oncol.*, vol. 113, no. 3, pp. 495–503, May 2013.

[8] A. N. Guthkelch et al., "Treatment of malignant brain tumors with focused ultrasound hyperthermia and radiation: Results of a phase I trial," *J. Neuro-Oncol.*, vol. 10, no. 3, pp. 271–284, Jun. 1991.

[9] S. Curto, A. Garcia-Miquel, M. Suh, N. Vidal, J. M. Lopez-Villegas, and P. Prakash, "Design and characterisation of a phased antenna array for intact breast hyperthermia," *Int. J. Hyperthermia*, vol. 34, no. 3, pp. 250–260, Apr. 2018.

[10] J. Li et al., "A preclinical system prototype for focused microwave breast hyperthermia guided by compressive thermoacoustic tomography," *IEEE Trans. Biomed. Eng.*, vol. 68, no. 7, pp. 2289–2300, Jul. 2021.

[11] M. Asili et al., "Flexible microwave antenna applicator for chemo-thermotherapy of the breast," *IEEE Antennas Wireless Propag. Lett.*, vol. 14, pp. 1778–1781, 2015.

[12] M. M. Paulides, J. F. Bakker, N. Chavannes, and G. C. Van Rhoon, "A patch antenna design for application in a phased-array head and neck hyperthermia applicator," *IEEE Trans. Biomed. Eng.*, vol. 54, no. 11, pp. 2057–2063, Nov. 2007.

[13] R. Gaffoglio, M. Righero, G. Giordanengo, M. Zucchi, and G. Vecchi, "Fast optimization of temperature focusing in hyperthermia treatment of sub-superficial tumors," *IEEE J. Electromagn., RF Microw. Med. Biol.*, vol. 5, no. 3, pp. 286–293, Sep. 2021.

[14] T. Deng, "Optimization of SAR distributions in liver and lung regions irradiated by the H-horn annular phased array hyperthermia system," *IEEE Trans. Microw. Theory Techn.*, vol. 39, no. 5, pp. 852–856, May 1991.

[15] R. Poni, E. Neufeld, M. Capstick, S. Bodis, and N. Kuster, "Rapid SAR optimization for hyperthermic oncology: Combining multi-goal optimization and time-multiplexed steering for hotspot suppression," *Int. J. Hyperthermia*, vol. 39, no. 1, pp. 758–771, Dec. 2022.

[16] P. Takook, M. Persson, and H. D. Trefná, "Performance evaluation of hyperthermia applicators to heat deep-seated brain tumors," *IEEE J. Electromagn., RF Microw. Med. Biol.*, vol. 2, no. 1, pp. 18–24, Mar. 2018.

[17] H. Nan, S. Liu, G. J. Buckmaster, and A. Arbabian, "Beamforming microwave-induced thermoacoustic imaging for screening applications," *IEEE Trans. Microw. Theory Techn.*, vol. 67, no. 1, pp. 464–474, Jan. 2019.

[18] M. J. Burfeindt, E. Zastrow, S. C. Hagness, B. D. Van Veen, and J. E. Medow, "Microwave beamforming for non-invasive patient-specific hyperthermia treatment of pediatric brain cancer," *Phys. Med. Biol.*, vol. 56, no. 9, pp. 2743–2754, May 2011.

[19] K. R. Mahmoud and A. M. Montaser, "Design of hyperthermia applicator to heat multi-brain tumors simultaneously based on adaptive beamforming technique," *IEEE J. Electromagn., RF Microw. Med. Biol.*, vol. 5, no. 2, pp. 115–123, Jun. 2021.

[20] J. Redr et al., "Microwave hyperthermia of brain tumors: A 2D assessment parametric numerical study," *Sensors*, vol. 22, no. 16, p. 6115, Aug. 2022.

[21] M. Zanoli, E. Ek, and H. D. Trefná, "Antenna arrangement in UWB helmet brain applicators for deep microwave hyperthermia," *Cancers*, vol. 15, no. 5, p. 1447, Feb. 2023.

[22] M. J. Hajiahmadi, R. Faraji-Dana, and C. Caloz, "Metasurface-based time-reversal focusing for brain tumor microwave hyperthermia," *IEEE Trans. Antennas Propag.*, vol. 70, no. 12, pp. 12237–12246, Dec. 2022.

[23] Z. Xi, X. Wang, K. Ye, and X. Wang, "Performance evaluation of focused microwave brain hyperthermia guided by microwave-induced thermoacoustic tomography," *IEEE J. Electromagn., RF Microw. Med. Biol.*, vol. 7, no. 4, pp. 383–391, Dec. 2023.

[24] D. B. Rodrigues, J. Ellsworth, and P. Turner, "Feasibility of heating brain tumors using a 915 MHz annular phased-array," *IEEE Antennas Wireless Propag. Lett.*, vol. 20, pp. 423–427, 2021.

[25] X. He, W. Geyi, and S. Wang, "A hexagonal focused array for microwave hyperthermia: Optimal design and experiment," *IEEE Antennas Wireless Propag. Lett.*, vol. 15, pp. 56–59, 2016.

[26] E. Zastrow, S. C. Hagness, and B. D. Van Veen, "3D computational study of non-invasive patient-specific microwave hyperthermia treatment of breast cancer," *Phys. Med. Biol.*, vol. 55, no. 13, pp. 3611–3629, Jun. 2010.

[27] P. T. Nguyen, A. M. Abbosh, and S. Crozier, "3-D focused microwave hyperthermia for breast cancer treatment with experimental validation," *IEEE Trans. Antennas Propag.*, vol. 65, no. 7, pp. 3489–3500, Jul. 2017.

[28] M. Franckena et al., "Radiotherapy and hyperthermia for treatment of primary locally advanced cervix cancer: Results in 378 patients," *Int. J. Radiat. Oncol. Biol. Physics*, vol. 73, no. 1, pp. 242–250, Jan. 2009.

[29] N. R. Datta et al., "Local hyperthermia combined with radiotherapy and-/or chemotherapy: Recent advances and promises for the future," *Cancer Treatment Rev.*, vol. 41, no. 9, pp. 742–753, Nov. 2015.

[30] P. A. Hasgall et al., "IT'IS database for thermal and electromagnetic parameters of biological tissues," Version 4.0, Tech. Rep., May 2018.

[31] L. Xu and X. Wang, "Focused microwave breast hyperthermia monitored by thermoacoustic imaging: A computational feasibility study applying realistic breast phantoms," *IEEE J. Electromagn., RF Microw. Med. Biol.*, vol. 4, no. 2, pp. 81–88, Jun. 2020.

[32] J. Stang, M. Haynes, P. Carson, and M. Moghaddam, "A preclinical system prototype for focused microwave thermal therapy of the breast," *IEEE Trans. Biomed. Eng.*, vol. 59, no. 9, pp. 2431–2438, Sep. 2012.

[33] P. T. Nguyen, A. Abbosh, and S. Crozier, "Three-dimensional microwave hyperthermia for breast cancer treatment in a realistic environment using particle swarm optimization," *IEEE Trans. Biomed. Eng.*, vol. 64, no. 6, pp. 1335–1344, Jun. 2017.

[34] G. Schooneveldt et al., "Hyperthermia treatment planning including convective flow in cerebrospinal fluid for brain tumour hyperthermia treatment using a novel dedicated paediatric brain applicator," *Cancers*, vol. 11, no. 8, p. 1183, Aug. 2019.

[35] A. T. Mobashsher, A. M. Abbosh, and Y. Wang, "Microwave system to detect traumatic brain injuries using compact unidirectional antenna and wideband transceiver with verification on realistic head phantom," *IEEE Trans. Microw. Theory Techn.*, vol. 62, no. 9, pp. 1826–1836, Sep. 2014.

[36] D. O. Rodriguez-Duarte, J. A. T. Vasquez, R. Scapaticci, L. Crocco, and F. Vipiana, "Brick-shaped antenna module for microwave brain imaging systems," *IEEE Antennas Wireless Propag. Lett.*, vol. 19, no. 12, pp. 2057–2061, Dec. 2020.

[37] M. Lazebnik, E. L. Madsen, G. R. Frank, and S. C. Hagness, "Tissue-mimicking phantom materials for narrowband and ultrawideband microwave applications," *Phys. Med. Biol.*, vol. 50, no. 18, pp. 4245–4258, Aug. 2005.

[38] Y. Yuan et al., "A heterogeneous human tissue mimicking phantom for RF heating and MRI thermal monitoring verification," *Phys. Med. Biol.*, vol. 57, no. 7, pp. 2021–2037, Mar. 2012.

[39] M. Ahmed, C. L. Brace, F. T. Lee, and S. N. Goldberg, "Principles of and advances in percutaneous ablation," *Radiology*, vol. 258, no. 2, pp. 351–369, Feb. 2011.

[40] S. N. Goldberg, G. S. Gazelle, and P. R. Mueller, "Thermal ablation therapy for focal malignancy: A unified approach to underlying principles, techniques, and diagnostic imaging guidance," *Amer. J. Roentgenol.*, vol. 174, no. 2, pp. 323–331, Feb. 2000.

[41] J. Li, L. Xu, and X. Wang, "A computational study on number of elements in antenna array for focused microwave breast hyperthermia," in *IEEE MTT-S Int. Microw. Symp. Dig.*, May 2019, pp. 1–3.

[42] C. Li et al., "Deep-learning-enabled microwave-induced thermoacoustic tomography based on ResAttU-net for transcranial brain hemorrhage detection," *IEEE Trans. Biomed. Eng.*, vol. 70, no. 8, pp. 2350–2361, Aug. 2023.

[43] Z. Luo et al., "Quantitative reconstruction of dielectric properties based on deep-learning-enabled microwave-induced thermoacoustic tomography," *IEEE Trans. Microw. Theory Techn.*, vol. 71, no. 6, pp. 2652–2663, Jun. 2023.

[44] J. Zhang, C. Li, W. Jiang, Z. Wang, L. Zhang, and X. Wang, "Deep-learning-enabled microwave-induced thermoacoustic tomography based on sparse data for breast cancer detection," *IEEE Trans. Antennas Propag.*, vol. 70, no. 8, pp. 6336–6348, Aug. 2022.

[45] O. Lorton et al., "Self-scanned HIFU ablation of moving tissue using real-time hybrid U.S.-MR imaging," *IEEE Trans. Biomed. Eng.*, vol. 66, no. 8, pp. 2182–2191, Aug. 2019.

[46] L.-W. Kuo, G.-C. Dong, C.-C. Pan, S.-F. Chen, and G.-S. Chen, "An MRI-guided ring high-intensity focused ultrasound system for noninvasive breast ablation," *IEEE Trans. Ultrason., Ferroelectr., Freq. Control*, vol. 67, no. 9, pp. 1839–1847, Sep. 2020.

[47] M. M. Paulides et al., "A printed Yagi–Uda antenna for application in magnetic resonance thermometry guided microwave hyperthermia applicators," *Phys. Med. Biol.*, vol. 62, no. 5, pp. 1831–1847, Feb. 2017.

[48] T. Drizdal et al., "Simulation guided design of the MRcollar: A MR compatible applicator for deep heating in the head and neck region," *Int. J. Hyperthermia*, vol. 38, no. 1, pp. 382–392, Jan. 2021.